Atmos. Meas. Tech. Discuss., 4, 2827–2881, 2011
www.atmos-meas-tech-discuss.net/4/2827/2011/
doi:10.5194/amtd-4-2827-2011


Atmospheric Measurement Techniques Discussions



# Early in-flight detection of $SO_2$ via Differential Optical Absorption Spectroscopy: a feasible aviation safety measure to prevent potential encounters with volcanic plumes

**L. Vogel[1], B. Galle[2], C. Kern[1,*], H. Delgado Granados[3], V. Conde[2], P. Norman[2], S. Arellano[2], O. Landgren[2], P. Lübcke[1], J. M. Alvarez Nieves[3], L. Cárdenas Gonzáles[4], and U. Platt[1]**

[1]Institute of Environmental Physics, University Heidelberg, Heidelberg, Germany
[2]Department of Earth and Space Sciences, Chalmers University of Technology, Gothenburg, Sweden



[3]Instituto de Geofísica, UNAM, Mexico D. F., Mexico
[4]Centro Nacional de Prevención de Desastres, Mexico D. F., Mexico
[*]now at: Cascades Volcano Observatory, US Geological Survey, Vancouver, WA, USA

Received: 5 May 2011 – Accepted: 9 May 2011 – Published: 16 May 2011

Correspondence to: L. Vogel (leif.vogel@iup.uni-heidelberg.de)

Published by Copernicus Publications on behalf of the European Geosciences Union.

**Abstract**

Volcanic ash constitutes a risk to aviation, mainly due to its ability to cause jet engines to fail. Other risks include the possibility of abrasion of windshields and potentially serious damage to avionic systems. These hazards have been widely recognized since the early 1980s, when volcanic ash provoked several incidents of engine failure in commercial aircraft. In addition to volcanic ash, volcanic gases also pose a threat. Prolonged and/or cumulative exposure to sulphur dioxide ($SO_2$) or sulphuric acid ($H_2SO_4$) aerosols potentially affects e.g. windows, air frame and may cause permanent damage to engines. $SO_2$ receives most attention among the gas species commonly found in volcanic plumes because its presence above the lower troposphere is a clear proxy for a volcanic cloud and indicates that fine ash could also be present.

Up to now, remote sensing of $SO_2$ via Differential Optical Absorption Spectroscopy (DOAS) in the ultraviolet spectral region has been used to measure volcanic clouds from ground based, airborne and satellite platforms. Attention has been given to volcanic emission strength, chemistry inside volcanic clouds and measurement procedures were adapted accordingly. Here we present a set of experimental and model results, highlighting the feasibility of DOAS to be used as an airborne early detection system of $SO_2$ in two spatial dimensions. In order to prove our new concept, simultaneous airborne and ground-based measurements of the plume of Popocatépetl volcano, Mexico, were conducted in April 2010. The plume extended at an altitude around 5250 m above sea level and was approached and traversed at the same altitude with several forward looking DOAS systems aboard an airplane. These DOAS systems measured $SO_2$ in the flight direction and at ±40 mrad (2.3°) angles relative to it in both, horizontal and vertical directions. The approaches started at up to 25 km distance to the plume and $SO_2$ was measured at all times well above the detection limit. In combination with radiative transfer studies, this study indicates that an extended volcanic cloud with a concentration of $10^{12}$ molecules $cm^{-3}$ at typical flight levels of 10 km can be detected unambiguously at distances of up to 80 km away. This range provides



enough time (approx. 5 min) for pilots to take action to avoid entering a volcanic cloud in the flight path, suggesting that this technique can be used as an effective aid to prevent dangerous aircraft encounters with potentially ash rich volcanic clouds.

## 1 Introduction

Volcanic gaseous emissions are typically composed of carbon dioxide ($CO_2$), water vapour, sulphur dioxide ($SO_2$), and halogen compounds. Depending on the conditions the plumes/clouds can also contain large amounts of ash (i.e. small, solid particles). A series of life threatening encounters of aircraft with ash-loaded volcanic clouds in the 1980s highlighted the risk of volcanic emissions to aviation. The main threat is posed by volcanic ash (Miller and Casadevall, 2000; ICAO, 2007; Prata and Tupper, 2009, and references therein), which may lead to engine failure via flame-outs if allowed to enter high temperature jet engines. Severe incidents were reported from Mt. St. Helens 1980, where a Lockhead C-130 lost two of its four turboprop engines; in the 1982 eruption of Galunggung, Indonesia, two Boing 747 lost power in one case of all four, in the other of three out of four engines at 11 300 m and 9000 m above sea level (a.s.l.), respectively. The crew of both airplanes managed to restart enough engines to make a safe landing at nearby airports, but only after descending several kilometres. A similar encounter occurred in 1989, when a Boing 747 flew into the cloud from nearby Redoubt volcano, Alaska, and lost power of all of its four engines (Casadevall, 1994). Also in this case, the crew managed to restart the engines one or two minutes prior to impact on the ground. Fortunately only economic losses resulted from these encounters and no human lives were lost. The eruption of Mt. Pinatubo 1991 resulted in more than 40 incidents, but none as dramatic as the above-mentioned ones. Nevertheless, damage to aircraft as a result of the Mt. Pinatubo eruption were estimated to exceed US$ 100 million (Miller and Casadevall, 2000).

Even encounters with volcanic clouds of relatively low ash and $SO_2$ content may have severe consequences to aircraft. Grindle and Burcham (2003) describe an incident in

August 2000, where a DC-8-72 research airplane of NASA flew into a volcanic cloud of Hekla volcano, Iceland. The presence of a volcanic plume was only verified afterwards by the scientific in-situ instruments on-board the airplane. No signs of a volcanic cloud were perceived by the crew. Although no damage was revealed by a first visual inspection of the engines, a later inspection showed that significant damage to the engines had occurred with clogged cooling passages of turbine blades and $SO_2$ in the engine oil. It was estimated that the remaining lifetime of certain vital parts of the engine was likely reduced to only about 100 h.

The incidents described above resulted from the melting point of volcanic ash (≈1100 K) being below typical operational temperature (1400 K) of jet engines if thrust is above idle. This can lead to clogging and accumulation of molten debris in the hotter part of the engine and its consequent loss of power. Other effects include clogging of cooling mechanisms which greatly reduces the engines' lifetime, and abrasion of engine parts. Next to its effects to the engines, the abrasive properties of volcanic ash can damage the outer hull of aircraft, avionic systems e.g. pitot-static tubes and abrade windscreens to the point of becoming opaque. Besides volcanic ash, certain volcanic gases can also be hazardous to aviation, especially sulphur dioxide $SO_2$ and sulphuric acid $H_2SO_4$. Although they do not impair the airworthiness of an aircraft in such drastic ways as volcanic ash, prolonged exposure might reduce the lifetime of aircraft systems and lead to costly repairs and ground time of the aircraft (ICAO, 2007).

One of the latest volcanic eruptions severely impacting commercial aviation was the April/May 2010 eruption of Eyjafjallajökull in April 2010 with a volcanic cloud being blown over Europe. Most of European airspace was closed for up to several weeks and although no life-threatening encounters occurred, economic losses are estimated to range up to € 2.5 billion for the airline industry alone (Zehner, 2010). This eruption demonstrated the vulnerability of modern societies to volcanic hazards. In the course of the Eyjafjallajökull crisis, the "no-fly-rule", which states that aircraft are not allowed to fly through volcanic clouds of any ash concentration, was replaced by conditional flying zones. The "No Fly Zone" encompasses areas with ash concentration higher than $2 \times 10^{-3}$ g m$^{-3}$ and the "Enhanced Procedures Zone", where volcanic ash concentrations are predicted to be between $2 \times 10^{-4}$ and $2 \times 10^{-3}$ g m$^{-3}$. This more flexible approach was meant to keep European air-traffic operational, but also has the risk of reduced life times of aircraft parts. Also, this new approach places new and more demanding necessities for modelling on the volcanic advisory centres (VAACs), because a much more detailed initiation of models, knowledge of source terms, and incorporation of all physical processes are necessary (ADF, 2010).



Commercial carriers rely on the volcanic ash advisory centrers (VAACs) of the International Airways Volcano Watch (IAVW) for volcanic cloud warnings and predicted locations of these clouds (Romero, 2004; ICAO, 2007). The VAACs use a wide set of observations and measurements, including ground based measurements from observing networks, special air-reports from pilots and observations from satellites (meteorological and non-meteorological). Most active volcanoes are not routinely monitored. Even if they are in remote locations, they can be in close proximity to busy air routes e.g. the Aleutian islands (Kasatochi volcano) and volcanoes in Kamchatka for trans-Pacific air routes. Furthermore, volcanic ash ejected into higher atmospheric layers can be rapidly dispersed over great distances (Prata, 2009), and eruption strength is not directly linked to ejection height (Tupper et al., 2009). Satellite based measurements of ash and $SO_2$ are thus the most important tool to detect volcanic clouds and eruptions (Prata, 2009; Thomas and Watson, 2010).

Ash detection from satellite platforms can be accurately performed in the infra-red (IR) spectral region. Retrievals are typically based on the "reverse absorption", the different absorption structures of water and ice versus ash in the 10 to 13 µm range, by taking the difference of these absorption structures ("brightness temperature difference (BTD) method", Prata, 1989; Wen and Rose, 1994). In recent years the addition of further channels in the retrievals has improved the detection limit and the ability to identify volcanic ash (e.g. Pavolonis et al., 2006; Pavolonis and Sieglaff, 2010; Clarisse et al., 2010; Thomas and Watson, 2010, and references therein). While pure ash clouds can be distinguished from water/ice clouds, mixed clouds are more difficult to separate.

Volcanic dust clouds can also be masked by "ordinary" meteorological clouds, and artefacts associated with dust or very cold cloud tops can cause false detections. These limitations have been discussed extensively and are known to the community (Prata, 1989; Rose et al., 1995; Simpson et al., 2000; Prata et al., 2001). With the introduction of high resolution instruments like Infrared Atmospheric Sounding Interferometer (IASI) and Atmospheric Infrared Sounder (AIRS), false ash detection induced by dust can be reduced significantly (Clarisse et al., 2010).

In the context of volcanic aviation hazards, $SO_2$ detection is used as a supplementary technique, because volcanic ash clouds are usually associated with $SO_2$ clouds of approximately equal size and location. $SO_2$ can be identify by its molecular absorption structures, both in the UV and IR spectral regions, the extent of a $SO_2$ cloud can serve as an indicator for areas affected by volcanic ash. Typically $SO_2$-levels in the free troposphere are very low (< 100 ppt above 2 km, Berglen et al., 2004), therefore there is only a very small background signal. Detection in the IR is mainly based on $SO_2$ absorptions bands around 7.3 µm (Prata et al., 2003; Prata and Bernardo, 2007), the 8.6 µm (Realmuto et al., 1994), and recently was combined with the 4 µm band (Karagulian et al., 2010). Remote sensing of $SO_2$ in the ultraviolet (UV) range is more sensitive and this region has been used since 1977 (COSPEC and later TOMS, see for instance Krueger, 1983). Today retrievals of $SO_2$ are based on Differential Optical Absorption Spectroscopy Technique (DOAS) (e.g. Platt and Stutz, 2008), and satellite-based $SO_2$ detection has proven very useful in detecting and tracking volcanic plumes in several cases in the past (Khokhar et al., 2005, 2008; Rix et al., 2009; Carn et al., 2009). Although reliable, the major drawback of volcanic $SO_2$ detection in the UV range is its limitation to daylight and limited coverage/overpass. Also, it can only be a proxy for the greater hazard, volcanic ash, which will fall out and might lead to two different clouds moving in different directions due to wind shear. However, for young clouds (up to three days after emission) $SO_2$ remains a good tracer for a volcanic cloud with dangerous ash contents (Carn et al., 2009; Guffanti et al., 2010; Schumann et al., 2011).



Detection of a volcanic eruption that potentially poses a danger to aviation should in the best case lead to a warning to aircraft within minutes. However, if the eruption goes unnoticed because the volcano is in a remote location, the weather conditions are unfavourable for satellite detection, or the satellite overpass misses it, several hours might pass before the thread is recognized and warning can be given. Thus already Prata et al. (1991) proposed an instrument on board aircraft to sense volcanic ash by its IR emission signature. A portable camera applicable for this purpose was presented in Prata and Bernardo (2009).

Although cameras for the detection of $SO_2$ based on two-wavelength detection in the UV range exist since 2006 (Mori and Burton, 2006; Dalton et al., 2009; Kantzas et al., 2010; Bluth et al., 2007; Kern et al., 2010a), reported detection limits reported to date are of the order of $10^{17}$ molec cm$^{-2}$ $SO_2$ slant column densities (SCDs) (Mori and Burton, 2006; Lübcke, 2010). This is not sufficient to detect expected $SO_2$ SCDs measured at greater distances to the volcanic cloud, as will be shown in this study. Remote sensing with the DOAS technique is more specific and offers better sensitivity than two-wavelength detection schemes.

In the following we will explore the feasibility of the DOAS technique as central component of an early in flight warning system of $SO_2$ and hence volcanic plumes. Prototype systems were tested, during a flight of a small airplane with forward looking DOAS instruments mounted. The volcanic plume of Popocatépetl was approached several times. Popocatépetl volcano is a suitable candidate for this test, because its summit is at a height of 5426 m (a.s.l.) while the elevation of the surrounding terrain is around 2000 m a.s.l. With the planetary boundary layer extending to an altitude of 2500–3000 m above ground (Doran et al., 1998), the plume disperses usually outside the planetary boundary layer at heights comparable to low flying commercial aircraft. Reported average emissions during April 2010 were of about 20 kg s$^{-1}$ (1730 Gg d$^{-1}$) according to the measurements of local monitoring stations from the Network for Observation of Volcanic and Atmospheric Change (NOVAC).

The paper is structured as follows: the general concept of an early in-flight detection system for $SO_2$ based on the DOAS technique is presented in Sect. 2. Section 3 describes the experimental setup used to proof the concept and the performed airborne measurements as well as additional ground based measurements. Also, the retrieval of $SO_2$ from gathered spectra is given. Radiative transfer studies performed with the conditions at hand are introduced. Subsequently, the results are discussed in Sect. 4. Experimental data is compared with radiative transfer studies to infer the maximum distance for detecting $SO_2$ in Sect. 5. The results of this study are concluded in Sect. 6. An analytical description of the expected decrease of $SO_2$ signal with distance is derived in Appendix A.

## 2 Early in-flight detection of $SO_2$ via Differential Optical Absorption Spectroscopy

Airborne DOAS measurements are routinely performed from various research aircraft. A recent examples from CARIBIC (Civil Aircraft for Regular Investigation of the atmosphere Based on an Instrument Container) of observations of volcanic plumes are described in Heue et al. (2011), which measured volcanic clouds originating from Kasatochi, 2008, and Eyjafjallajökull, 2010. Different trace gases could be identified (BrO, $SO_2$). These measurements were performed with sideways looking instruments and interest was focused on satellite validation and plume chemistry. Here, we explicitly study the capabilities of a forward looking DOAS instrument as an early warning system for $SO_2$.

Figure 1 illustrates the $SO_2$ signal to be expected from a forward looking telescope mounted in an airplane. In the upper part, it shows as sketch of the observation geometry for a forward looking telescope in an aircraft approaching a volcanic plume and in the lower part the expected $SO_2$ slant column densities (SCDs) for an airborne approach traversing through the plume as well for a ground-based, upward looking instrument (e.g. an instrument mounted on a car) traversing beneath the plume. A



gaussian distribution of the $SO_2$ concentration in the plume is assumed. Also indicated are three regimes for airborne approaches: A – the plume only partly fills the field of view (FOV) of the instrument, B – the plume completely fills the FOV, C – the measurements are performed inside the plume. In regime A there is a strong increase of the $SO_2$ SCD with decreasing distance to the plume for two reasons, (1) as the instrument approaches the plume it continues to fill a larger part of the FOV, thus (2) less radiation is scattered into the FOV between the instrument and the plume. The radiation from the FOV not having penetrated the plume does not carry the $SO_2$ absorption signature, thus, both effects will lead to increase of the $SO_2$ optical density seen by the instrument at smaller distances to the plume. Once the volcanic plume fills the FOV of the instrument (regime B), increase in $SO_2$ absorption structure with decreasing distance should follow an exponential increase with a subsequent drop in retrieved $SO_2$ signal inside the plume. It is interesting to note that (for an optically thin plume with little multiple scattering inside) the airborne measurements will see the maximum $SO_2$ SCD when the aircraft (and thus the instrument) reaches the front edge of the plume. Ground-based instruments will see the maximum $SO_2$ SCD when the instrument is just below the plume centre. As our radiative transfer study (Sect. 3.4) and measured data (Sect. 3) show in this study, the exact gradient seen by an instrument inside the plume depends on the aerosol load at hand. Also, the maximum $SO_2$ SCD might be perceived not at the edge but further inwards in the plume for airborne approaches.

In order to take evasive measures and prevent an encounter of the aircraft with a volcanic cloud, the above described approach of an instrument looking along the direct flight vector needs to be extended to resolve the plume spatially. This is easily achieved by additional instruments with viewing directions along a horizontal and vertical offset to the flight vector. In the best case this would result in displaying a two dimensional distribution of $SO_2$ SCDs in the direction of flight of the aircraft (see Sect. 3), allowing to circumvent areas of increased $SO_2$ concentration and minimizing the chance to encounter volcanic ash by evasive action.

An additional radiative transfer study was conducted to reproduce the measurements, extrapolate found dependencies to greater distances and infer the limit of detectability of the plume.

## 3 Experimental setup

In order to provide experimental proof of our concept for a DOAS-based early warning system, we performed measurements on board a small airplane probing the plume of Popocatépetl volcano, Mexico, on 24 April 2010. As mentioned above, Popocatépetl is especially well suited for studies on the detection of $SO_2$ from airplanes due to (1) its high altitude of 5426 m a.s.l. and its relatively high $SO_2$ emission flux. Moreover (2), Popocatépetl is one of the volcanoes, which are equipped with ground-based DOAS instrumentation for continuous monitoring of the $SO_2$ emission flux within the NOVAC network (Galle et al., 2010), thus independent measurements of the $SO_2$ emission were available, which were – according to the ground-based network – around 1900 Gg day$^{-1}$ during the time of our measurements. Also, plume height and direction were monitored by two additional ground based stationary scanning instruments and conventional car traverses of the plume were conducted with a zenith sky looking DOAS instrument. (3) These flights provided a largely realistic simulation of an encounter with an arbitrary volcanic plume in the troposphere outside of the planetary boundary layer (PBL) as e.g. encountered during the Eyjafjallajökull eruption over Europe during April and May 2010.

The meteorological conditions were stable with clear visibility at flight altitude for all approaches. An open cloud cover well above the plume was present as well as a slight haze in the boundary layer below.

The airborne measurements were conducted with a Cessna 421, on which three telescopes were installed next to the window of the copilot. One telescope was pointing directly forward at 0 mrad elevation angle, where as the other two were dual beam telescopes similar to the ones described in Johansson et al., 2009. Each dual



beam telescope has two viewing directions separated by 80 mrad (4.6°). These telescopes were aligned such that they were pointing 40 mrad (2.3°) towards port and starboard and 40 mrad above and below the central viewing direction, respectively (Fig. 2). Each of the tree telescopes was connected to a spectrometer (or two in the case of the dual beam telescopes) with which the incident light was spectrally analysed. The fibre from the centre looking telescope was connected to a high grade spectrograph (QE65000, Ocean Optics), light from the sideways looking dual-beam telescopes was analysed with dual spectrograph of type S2000 (Ocean Optics) with (compared to the QE65000 instrument) somewhat lower resolution and higher noise (Table 1). The field of view (FOV) for all five viewing directions was 8 mrad (0.46°). In this way, the setup was able not only to detect the volcanic plume but also gather information on its spatial extent. The instrumental setup was very compact with telescopes of size 115 mm × 40 mm (length × diameter) and spectrograph dimensions (length × width × height) of 141.6 mm × 104.9 mm × 40.9 mm (S2000) and 182 mm × 110 mm × 47 mm (QE65000).

### 3.1 Airborne measurements

In total, six approaches towards and subsequent traverse through the volcanic plume were made between 16:00 h and 17:15 h UTC. They are labelled I till VI in Fig. 3. Further information on average altitude a.s.l. and direction of approach [azimuth °N] are given in Table 2. The azimuth and elevation angles were calculated from the GPS data recorded on board the aircraft. Thus both values represent viewing direction based on the difference between two subsequent locations of measurement and can only be approximates for the planes orientations yaw, pitch and actual viewing direction of the telescopes.

The purpose of approaches I and II was to gather information about the plume altitude and to test the instrumental setup before going to greater distances from the plume. Like approach VI, they are not well suited for studying the detectability of $SO_2$ due to the encounter of strong inhomogeneities in the plume, or since the aircraft flew

at the wrong altitude and/or changes in flight course had to be made. The effect of a misaligned approach of the plane can be seen e.g. in approach II, where a change in the plane's approach elevation angle was associated with a sudden increase in the $SO_2$ column density measured by the central DOAS instrument (Fig. 8). While this approach can not be used to study DOAS as an early detection technique of $SO_2$ it still allows comparison with the car traverse (Sect. 4.1). Approaches III, IV and V were conducted starting at larger distance to the plume and will be discussed in detail in the following. Due to air space restrictions the maximum distance to the plume achieved at the start of an approach was only 25 km or less. To draw conclusions about the maximum distance at which $SO_2$ from the plume might still be detected, the measurements need to be extrapolated using theoretical considerations (Appendix A) as well as radiative transfer model studies (Sect. 5).

### 3.2 Ground based measurements

Further measurements were conducted from the ground to provide plume altitude and wind direction. These parameters were communicated to the airplane via radio link. A zenith pointing DOAS instrument was mounted on a car and used to conduct traverse measurements under the plume between 8 and 14 km distance to the crater, yielding location and extent of the plume as well as wind direction (Fig. 4). Because of road conditions and construction along the way, traversing the plume generally took about one hour. Also, the plume was not blown perpendicular to the road. Calculation of fluxes and wind direction was performed using the MobileDOAS software package (Zhang and Johansson).

Additionally, two stationary DOAS instruments were deployed on both edges of the plume (Fig. 4), allowing to approximate wind direction as well as the plume altitude. The instrumental design is analogue to the NOVAC instrument Version I as described in Galle et al. (2010). They scan the volcanic plume along a 60° cone, which is a routinely performed volcanic gas emission measurement technique in the NOVAC network. Calculation of plume height and direction was also performed with the NOVAC



software package. The stationary instruments had the advantage of a higher time resolution (≈10 min per scan) than the traverses.

### 3.3 The DOAS retrieval

All gathered spectra were evaluated using the DOASIS software package from the Institute for Environmental Physics, Heidelberg, Germany (Doasis; Kraus, 2006; Lehmann, 2011). The program applies a combination of a non-linear Levenberg-Marquardt and a standard least-squares fit to determine the optical density of trace gas absorption (Platt and Stutz, 2008). Absorption cross sections of the following species were included in the fit: $SO_2$ at 273 K (Bogumil et al., 2003) and $O_3$ at 280 K (Voigt et al., 2001), both chosen for their close vicinity to ambient temperature at the flight height. In addition to $SO_2$ and $O_3$, also a clear sky reference (CSR) spectrum and a Ring spectrum (Solomon et al., 1987) were fitted. The latter was calculated from the CSR with the software DOASIS. Broad band absorptions and Mie scattering were accounted for by using a polynomial of 3rd order and a wavelength-independent offset was included to correct for possible stray light. All spectra collected were evaluated in the wavelength range between 307.4–317.8 nm. For all instruments and approaches of the airborne measurements, CSR spectra were constructed from 10 consecutively recorded spectra, measured after the plane had passed the plume but still continued on the same course. Thus the CSR was recorded under as similar as possible illumination conditions as the actual measurements and in close temporal proximity. The CSR was wavelength calibrated by comparison to a high resolution solar spectrum (Kurucz, 2005), which was convoluted with the respective instrumental slit function. The obtained calibrations were transferred to all other spectra of corresponding approach and instrument. The ambient temperature at flight altitude was approximately −1 °C according to data from the READY NOAA model (READY) at 500 mbar or 5120 m a.s.l. at the time of the flight on 24 April 2010.

Note that in contrast to previous radiative transfer studies (Mori et al., 2006; Kern et al., 2010b), here we do not aim to retrieve correct $SO_2$ SCDs but intent only to

study the gradient of the $SO_2$ signal with distance to the plume. Thus the evaluation of gathered data in this fit range most sensitive to $SO_2$ is justified. A correction factor of 2 was used to calculate the measurement error from the fit error according to (Platt and Stutz, 2008) based on residual structures and $SO_2$ absorption band widths. The mean measurement error is determined from all measurements gathered at distances greater than 10 km for approaches III–V of the respective instrument (Table 1). This ensures that the for the study relevant error is given.

### 3.4 Radiative transfer modelling

Several model scenarios were set up in the 3-D radiative transfer model McArtim (Deutschmann, 2008; Deutschmann et al., 2011), successor of the model TRACYII (Wagner et al., 2007), to assess the sensitivity of DOAS measurements of $SO_2$ to the distance between the instrument and the plume and on the wavelength of the measurement. Figure 1 depicts the model setup schematically and effects influencing the measured absorption signal.

Two different types of model runs were conducted with the radiative transfer model. Type A model runs were set up in an attempt to match the conditions observed during the measurements at Popocatépetl. Afterwards, type B model runs were conducted to examine the differences that might be encountered when flying towards a volcanic cloud of much larger extent, as might be the case after a large-scale volcanic eruption.

For both types of model runs, the ambient atmosphere contained a typical $O_3$ layer with a maximum concentration of $5 \times 10^{12}$ molec cm$^{-3}$ at 22 km altitude and total column of $9 \times 10^{18}$ molec cm$^{-2}$ ($\approx$ 330 DU), as this influences the atmospheric radiative transfer in the ultraviolet wavelength region. A 30° solar zenith angle was assumed for the calculations. All aerosol particles were characterized as purely scattering with a single scattering albedo of 1 and a Heyney-Greenstein asymmetry parameter of 0.8, which is typical for scattering sulphate aerosols. For all simulations, the instrument was located at the same altitude as the plume centre, and was aimed with a narrow field of view (0.3°) in horizontal direction towards the centre of the plume. Note that both



model run types assume a plume which has no concentration gradient from centre to its edges.

#### 3.4.1 Model runs type A: spaciously confined plume with different aerosol contents.

In these model runs, the measurement geometry and atmospheric conditions were initialized using the conditions observed during the measurement at Popocatépetl. The volcanic plume was simulated with a centre at 5.5 km altitude, a height of 2 km, a horizontal width of 6.5 km and infinite length.

With these boundary conditions, several model runs were performed with variations of the plume's $SO_2$ concentration and aerosol extinction coefficient (AEC), given in Table 3. For model runs A1 and A2, the $SO_2$ concentration would result in a measured SCD of $1 \times 10^{18}$ molec cm$^{-2}$ if measured from the edge of the plume without occurrence of multiple scattering. For model run A3 the $SO_2$ concentration was reduced in order to reproduce column densities similar to those observed in the aircraft measurements.

#### 3.4.2 Model run B: large scale $SO_2$ clouds.

This scenario has been chosen to model the response of the proposed technique to volcanic clouds, as they might occur after large scale volcanic eruptions. Once the volcanic plume has travelled a large distance from the volcano, its horizontal dimensions are typically such that they considerably exceed the mean free photon path length in the atmosphere (several 10 km). In such cases, light entering a UV-spectroscopic instrument will not have passed through the entire volcanic cloud. To test the sensitivity of such instruments to large scale volcanic $SO_2$ clouds, model run B was set up using a $SO_2$ cloud with infinite extent in one horizontal direction. A $SO_2$ concentration of $1 \times 10^{12}$ molec cm$^{-3}$ was assumed for the simulation, and the cloud exhibited an aerosol optical density of 0.1 km$^{-1}$. Aerosols were considered to be purely scattering,

as is typical for sulphate aerosol. The cloud was modelled at 10 km. The results of this model run will be discussed in Sect. 5 to give an outlook on the base of the conducted measurements.

## 4 Results

### 4.1 Measurement results from airborne observations

All approaches successfully detected $SO_2$ from the first measurement of the approaches onwards, but restrictions in airspace prevented measurements at distances further than 25 km from the plume. Figure 6 depicts the $SO_2$ column densities as a function of distance from the plume centre for approaches III through V for the different viewing directions. The mean error $\sigma$ for a measurement is specified in Table 1 (see Sect. 3.3). The result of the retrieval for the spectrum gathered at greatest distance to the plume (first spectrum of approach IV) is shown in Fig. 7.

#### 4.1.1 Measurement regimes and extent of plume

First, the $SO_2$ column time series are discussed. At 25 km distance to the plume, the FOV of each telescope corresponds to a circle of 200 m diameter at the plume, their centre being 2 km apart for the horizontal and vertical off-centred viewing directions, respectively. Thus it can be assumed that the centre, port and starboard looking telescopes started measuring in regime B (plume fills FOV), and the upwards and downwards looking telescopes started at regime B or in the transition from measurement regime A (plume partly fills FOV) to B. Due to the lower signal to noise ratio of the S2000 spectrograph (up, down, port, starboard telescope), a clear transition point can not be distinguished. In order to discuss the transition between regime B and C, the airborne approaches are best compared to ground based car traverses.

Approach II was performed approximately between 16:06 h–16:10 h UTC and compared with car traverse 2, which was measured from 15:34 h–16:05 h UTC. It can not



be used in the study on $SO_2$ detectability due to changes in flight altitude in the first minute. However, the plane did not change direction during the rest of approach II and while travelling through the plume. Due to its close proximity to the car traverses in space and time, it can be used to compare both measurements. For that purpose, the ground based measurements were interpolated onto the path of the airplane approach assuming a linear expansion from the source to each measurement point. The result is depicted in Fig. 8. The plume can be well approximated by a gaussian fitted to the car traverses, which sets the plume center at 0 km at the maximum of the gaussian.

Comparing airborne approach II and car traverse 2, the expected characteristics as argued in Sect. 2, Fig. 1, are clearly visible. The $SO_2$ SCD of the airborne measurements is increasing approximately until entering the plume, which horizontal distribution is captured by the car traverses. But it is also apparent, that the maximum $SO_2$ SCD of the airplane approach does occur almost, but not exactly at the edge of the plume rather is measured several hundred meters inside the plume. The model results discussed in Sect. 4.3 show that the retrieved $SO_2$ SCDs might change significantly with the transition from outside to inside the plume, with a shift of the maximum $SO_2$ SCD to the centre of the plume with increasing AEC. Thus the comparison between car traverse and airborne approach indicates that multiple scattering inside the plume causes the maximum column density to be measured within the plume, not at its front edge.

Airborne approaches III–V crossed the plume further downwind. Thus plume position and size can not be simply extrapolated from the ground based measurements to the location of the airborne measurements. Also, the exact plume position can only be approximated from airborne measurements applying only forward looking DOAS telescopes.

The exponential relationship (Eq. 2) between retrieved SCD and distance to source as derived in Appendix A, is only valid in regime B. Also, approximations made might not hold for higher $SO_2$ SCDs and in close proximity of the plume, in which light scattered into the viewing direction of the telescope might still be affected by absorption structures from the plume's gases. Thus regime C is approximated by fitting function

2 to the signal of the centre looking telescope for the far field of approaches III, IV and V. The start of regime C was set to the start of a steadily increasing difference ($> 2.5 \times 10^{16}$ molec cm$^{-2}$) between fitted curve and retrieved values. The end of the plume is reached when the $SO_2$ values are below the detection limit of the instrument. The so determined regime C is marked by the dashed vertical lines in Fig. 6.

#### 4.1.2 Spatial separability of the different viewing directions

The airplane was flying at the same altitude as the volcanic plume and approached it from the side. Although $SO_2$ was detected by all instruments from the first measurement onwards, significant differences between the retrieved SCDs of the telescopes can not be distinguished for measurements at greater distance to the plume. The signal-to-noise ratio of the Ocean Optics S2000 spectrometers used for the measurements with non-centre-looking telescopes was inferior to that of the QE65000 (centre-looking telescope). Thus the precision of the measurements done with the S2000 was not sufficient to detect differences in $SO_2$ column at large distances from the plume.

Theoretically, $SO_2$ SCDs measured in starboard, centre and port direction during the approach should not differ greatly for a homogeneous plume along its path of propagation. For the vertical viewing directions (down, centre, up), differences in signal should depend on the distance to the plume and its vertical extent. At some point close to the edge or inside the plume, the gradients of all instruments should coincide until the plume is passed (and afterwards showing no $SO_2$ signal), because the different telescopes are observing increasingly similar parts of the plume.

While the plane approaches, the upward and downward looking instruments start observing the plume and their gradients should increase and start converging to the gradient of the centre looking instrument, because the different telescopes are observing are increasingly similar parts of the plume. At some point at the edge or inside the plume, the gradients of all instruments should coincide until the plume is passed (and afterwards showing no $SO_2$ signal).



Comparing the horizontally sideways pointing telescopes, similar $SO_2$ gradients are observed at most times except for approach III, where a change in flight direction while inside the plume lead to a strong increase in the port signal (see also Fig. 3).

For the different vertical viewing directions, differences in the results obtained become more pronounced when the measurements are performed in and close to regime C. The telescope looking downwards always detects a significantly higher $SO_2$ SCD than the upwards looking telescope. Furthermore, it shows a comparable (Approach III and IV) or greater (Approach V) $SO_2$ SCD than the centre looking telescope. Possible issues discussed are (1) the plume was traversed above its centre altitude although results from the ground based measurements indicate that the plume's height was slightly above the plane's approach altitude (see Sect. 4.2). Changes in plume height due to e.q. Lee-waves cannot be ruled out, but as described above, the differences in optical path lengths inside the plume should become negligible closer to the plume. (2) A severe misalignment of telescopes; this can be ruled out, because even at greatest distances all telescopes observed the plume. (3) Strong small scale inhomogeneities of $SO_2$ concentrations inside the volcanic plume should be negligible due turbulences between source and measured plume section. (4) light detected by the downward looking telescope is subject to an increased path length inside the plume; this effect is certainly present but should only be of second order, because the telescopes are observing very similar plume cross sections as discussed above. (5) Errors in calibration and instrumental function for the different spectrograph should lead to additional structures in the residuum of the DOAS fit algorithm. This was not observed. A final conclusion is not possible because additional calibration quartz glass cells filled with $SO_2$ were not available to perform calibration and comparison of the different viewing directions.

Although early detection capabilities of DOAS for $SO_2$ could be proven, future studies are necessary with higher grade spectrometers for all viewing directions combined with additional calibration and instrument intercomparison. This includes additional modelling to assess radiative transfer effects for the different viewing directions.

### 4.2 The ground based measurements

The wind direction derived from automobile based measurements (the direction between the volcano's summit and the maximum encountered column densities) are depicted in Fig. 9. Both car traverses and the stationary ground-based instruments yield comparable wind directions with an average of 232° N. The small systematic differences between the results of the two methods might be explained by the different cross sections of the plume seen by each measurement technique. Also, the algorithm for the stationary instruments assumes that both instruments are measuring the same cross section of the plume. Regardless of these small systematic errors, the results clearly show the stability of meteorological conditions during the time of the airborne approaches. The altitude of the centre of the plume was calculated to be between 5250 and 5750 m a.s.l., the spread of plume heights can be explained by varying emission strengths and wind speeds. Stronger winds tend to press the plume slightly downwards in the proximity of the volcano. Given the summit height of 5426 m a.s.l., the retrieved plume heights correspond well to the visual observations of a plume at approximately the same or slightly lower altitude as Popocatépetl's summit.

Comparing the altitude of plume centre derived by the two stationary instruments with the altitude of airplane approaches, the plume's centre is generally measured about 200 m higher than the mean altitude of airplane approaches (5250 m a.s.l.). These measurements confirm that the airplane approaches were performed at the approximate plume height and during stable meteorological conditions.

### 4.3 Results from radiative transfer study

Here, model runs A will be discussed because they allow conclusions over the measurements. The reader is referred to Sect. 5 for the results of model run type B as an outlook on bases of the conducted experiment. As exemplary result of the model runs A, model run A2 is shown in Fig. 10. Its AEC was chosen, so that the gradients of measurements and model run A2 match qualitatively (see also Fig. 6). With an assumed



FOV of 5.2 mrad (0.3°), at the maximum distance modelled (100 km) a circle of diameter of ≈520 m is observed at the plume. Thus the all modelled approaches correspond to measurements in regime B and C.

In Fig. 10, the dependency of the measured $SO_2$ SCD on distance can be seen. The gradient of the retrieved $SO_2$ SCD follows the expected line with a clear separation of wavelengths. Longer wavelengths are less affected by Rayleigh scattering than smaller ones and thus less dependent on distance to the cloud. This leads to a difference in relative decrease of about a factor 10 at 100 km distance to the plume.

Studying the transition between simulated measurements in regime B and regime C (the plume is indicated as a grey shaded area), some interesting features are immediately visible: intuitively, one would suspect the maximum $SO_2$ signal just when the plane enters the plume, because light can no longer be scattered into the instrument's field of view without having passed the plume. This is reproduced by the model run A1 when low AEC is assumed. With increasing AEC in model runs A2 and A3 however, a shift to the centre of the plume becomes apparent of maximum SCDs. Also, a sharp edge can be seen in the SCD distribution at the position where the aircraft enters the plume (+3.25 km). This could be the explanation for the distribution observed in the measurement and the differences shown between car traverse and plane approach II (Fig. 8). Measurements taken at the front edge of the plume are not detecting radiation that has penetrated the entire plume, but rather measure light scattered by aerosols in the front portion of the plume. On the other hand, measurements taken inside the plume can be affected by significant enhancement of the light path inside the plume due to multiple scattering. Although the modelled cases are greatly simplified, e.g. a real plume is not evenly distributed over a discrete interval, they show that the maximum $SO_2$ column is not necessarily detected at the front edge of the plume. Thus, care must be taken when judging which spectra have been taken in and outside of the plume (regime B and C, respectively).

## 5 Comparing measurements to model results: inferring maximum distance at which $SO_2$ can be detected

To compare model results and measurements, an exponential function was fit to the different approaches. It is based upon a simplified determination of visibility and contrast that can be found in textbooks about radiation transport in the atmosphere (e.g. Platt and Stutz, 2008, p.110) and an analogue has been applied for radiative transfer corrections of UV-camera measurements in Bluth et al. (2007).

$$\frac{S(L_2)}{S(L_1)} \approx e^{-\epsilon \times (L_2 - L_1)} \quad (1)$$

The above function describes the relative change of retrieved SCD $S(L_1)$ and $S(L_2)$ between distance $L_1$ and $L_2$ to the plume. For a detailed derivation see Appendix A. $\epsilon$ is the total extinction coefficient depending on Rayleigh and Mie scattering, retrieval wavelength range and the distribution of absorption structure of the trace gas of interest in the respective retrieval wavelength range. Because the retrieved SCDs all possess a certain error, it is advantageous to use

$$S(L) = \mathrm{A} \times e^{-\epsilon \times L} \quad (2)$$

where A is a hypothetical SCD at zero distance or in our case the plume's centre. Function (2) is only valid for measurements taken in the regime B (see Fig. 1). Also, the "narrow beam" approximation must hold, thus light scattered into the viewing directions should not have passed the plume at an earlier point. In order to ensure these boundary conditions, only measurements taken more than 8 km from the assumed plume centre were used to retrieve the parameters of function (2) for the respective approaches.

The results for all fits are depicted in Fig. 11. They are extrapolated to 50 km distance to the plume. The individual obtained parameters are also shown in Table 4. The mean extinction coefficient $\epsilon$ returned by the fit was $7.33 \times 10^{-5}$, and the mean coefficient of determination $r^2$ was 0.94. Thus with the experimental setup, which was not specially



tuned for this kind of measurements, and a detection limit of $1.6 \times 10^{16}$ molec cm$^{-2}$ for the centre looking telescope (Table 1), the plume of Popocatépetl could have been detected from a distance greater than 35 km.

In order to compare the measurements to the modelled results, function 2 was fitted also to all model runs type A. The fit was performed between 10 and 100 km. The model runs are reproduced well by the analytical approach. All fits achieve a coefficient of determination ($r^2$) of more than 99.8 %. Table 5 summarizes the fitted extinction coefficients $\epsilon$ for 306.6 nm and 310.8 nm of model runs A1, A2 and A3. For model run A1 the fitted extinction coefficient is slightly increased in comparison to the other two. The reason is that model run A1 displays stronger absorptions at 10 km distance then the other two model runs. The approximation made in deriving function 2 are only valid for small absorptions and thus for model run A1 an additional systematic error is induced.

The extinction coefficients from the airborne approaches can be compared to the mean extinction coefficients obtained from the model runs. The relative decreases in SCDs calculated from the extinction coefficients of the approaches are encompassed between the mean results obtained for model runs A for 306.6 nm and 310.8 nm. The fitted $\epsilon$ of all approaches and their 95 % confidence bands are depicted together with the mean $\epsilon$ derived from the model runs A in Fig. 12. The differences between model and measurements can be explained by the wavelength interval used in the DOAS evaluation. The first and strongest absorption line in the DOAS retrieval interval 307.4–317.8 nm is the absorption maximum at 308.7 nm, influencing the DOAS retrieval heavily. Thus, it is consistent that the value of the extinction coefficient $\epsilon$ of the DOAS retrieval lies about halfway between the extinction coefficients of 306.6 nm and 310.8 nm of the modelled scenarios. These results validate the model runs and allow to extent the experimental "proof of concept" measurement with model run B.

**Early detection of an extensive volcanic cloud, results model run B**

As an example for the response of the proposed early detection system, an extensive volcanic cloud was simulated in model run type B. The result is shown in Fig. 13. The volcanic cloud was modelled with infinite horizontal extent and was located at 10 km altitude, a typical flight altitude for commercial airplanes. Note that in contrast to Fig. 10, the ordinate is displaying a logarithmic scale to enhance visibility of the gradients at large distances to the volcanic cloud. Again, a clear separation of retrieved $SO_2$ SCDs at different wavelength intervals with distance can be observed.

The relative changes in signal strength do not directly correspond to relative changes in detectability because the $SO_2$ absorption cross-section decreases with wavelength. The detection limit is instead given by the optical density obtained in a measurement, which is the product of the column density and the differential absorption cross-section. For model run B, the simulated optical density is depicted as a function of wavelength in Fig. 14. A typical DOAS instrument which has been tuned to the task might be able to resolve optical densities of about $10^{-3}$ at a measurement integration time of a few seconds. This limit is reached at 80–90 km distance to the volcanic cloud for the wavelength range 310–315 nm. Thus, given a slightly enhanced setup, there is a realistic option of a feasible early detection of a volcanic $SO_2$ cloud at these distances.

## 6 Conclusions

The measurements presented here clearly demonstrate the general applicability of DOAS as an early detection technique for $SO_2$ in a "proof of concept" campaign. A number of plume approaches were flown, and the measurement results were reproduced with a radiative transfer model. Although the approaches were only started at up to 25 km distance to the plume, the found relationship of signal to distance of the measurements could be used to extrapolate the experiment to 100 km distance. Due to the lower air pressure at typical flight altitudes (about 10 km) when compared to the



altitude of the Popocatépetl plume, additional radiative transfer studies conclude that a volcanic plume with a $SO_2$ slant column density of $10^{18}$ molecules $cm^{-2}$ as viewed from the outside can be detected at distances up to 80 km away. This range provides enough time for pilots to take actions to avoid plume fly-through under typical flight conditions, suggesting that this technique can be used as an effective aid to prevent dangerous aircraft encounters with potentially ash-laden volcanic plumes. But further efforts are needed in experiment and modelling to fully explore the capabilities of the technique. This includes the ability to spatially resolve volcanic plumes at greater distances in order to allow avoidance measures to be initiated, as well as a thorough investigations of the limitations e.g. in case of high altitude clouds between plume and instrument. Furthermore, the sensitivity to a volcanic cloud with ash particles covered in ice need to be addressed, because this is one of the cases were IR techniques based on the reverse absorption method are not suitable. Early detection possibility via DOAS would be reduced most likely, as this case is similar to type A model runs with an increased scattering aerosol content.

Large volcanic clouds are much more easily evaded by flying over or under them than by trying to go around them. Therefore, the vertical direction is arguably more important than the horizontal one. E.g. one could imagine a DOAS instrument applying an imaging spectrometer, which could be positioned so that its spatial axis is in the vertical, its dispersive axis is horizontal (IDOAS, Louban et al., 2009).

DOAS based $SO_2$ detection is a complementary technique to the detection of ash in the infra-red regime and in combination can greatly mitigate the risk from volcanic clouds to aviation.

## Appendix A

### Analytical approach to the radiation dilution effect

In general, the propagation of radiation in the atmosphere is a complex process. Multiple scattering inside and light dilution outside the plume both affect the measured signal. For a valid assessment of volcanic emissions both effects need to be taken into account. For this study, the gradient of measured $SO_2$ SCDs with distance between instrument and plume needs to be determined to assess the feasibility of DOAS as an early detection system for $SO_2$. The true concentrations inside the plume are only of secondary concern, and we focus only the radiation dilution.

An analytical solution can be derived to estimate the dependency of measured SCD to distance to the volcanic plume. The approach is analogous to the simplified determination of visibility and contrast that can be found in text books about radiation transport in the atmosphere (e.g. Platt and Stutz, 2008, , p.110). A similar strategy has been applied for radiative transfer corrections of UV-camera measurements in Bluth et al. (2007).

There, a black object of zero intensity is viewed from distance $L$ with a background intensity $I_0$ next to the object. Radiation scattered into the field of view of the observer will lead to an increase of the perceived intensity $I_R$ with increasing distance to the object until background intensity $I_0$ is reached. Certain approximations are made. (1) The probability is negligible that a photon is scattered into the viewing direction of the telescope after having been scattered out of it (Narrow Beam approximation). Consequently, extinction, which is comprised as the sum of Rayleigh and Mie scattering, can be treated like absorption as described by Lambert-Beer's Law. In our case it is the radiation scattered into the viewing direction. (2) The atmosphere is considered homogeneous. With these approximations, the scattered radiation intensity $I_R$ received by the observer when looking at a black object at distance $L$ is given by

$$I_R(\lambda) = I_0(\lambda) \times \left(1 - e^{-\epsilon(\lambda) \times L}\right) \tag{A1}$$



where the extinction coefficient $\epsilon(\lambda) = \epsilon_R(\lambda) + \epsilon_M(\lambda)$ is the sum of the Rayleigh and Mie extinction coefficients.

The wavelength dependency of Rayleigh and Mie scattering can be disregarded for a 1st order approximation of the dependency of DOAS retrieval on radiation dilution. Rayleigh scattering is approximately proportional to $\lambda^{-4}$, whereas Mie scattering has a wavelength dependency proportional to $\lambda^{-1.3}$. This results in a relative difference of scattered intensity of $\approx 18\,\%$ between 10 nm (wavelength range of DOAS retrievals) in the range of 300 nm and 330 nm. The evaluation of $SO_2$ is strongly dependent on the stronger differential optical absorption features at lower wavelengths (see Fig. 5). The difference between minima of the differential optical absorption cross sections of $SO_2$ is ($\approx 2$ nm). On this scale, the relative difference due to Rayleigh and Mie scattering is only $\approx 3\,\%$. Thus the error introduced by neglecting the wavelength dependency of Rayleigh and Mie scattering will be at the lower end of the interval 3 %–18 %.

Measured $SO_2$ SCDs (S) are proportional to the amplitude of its differential optical absorption structures:

$$S \propto ln\left(\frac{I_0}{I}\right) \tag{A2}$$

Taking the intensity of absorption minima as background intensity $I_0$ and absorption maxima as intensity $I$, a retrieved $SO_2$ SCD $S(L')$ will decrease with distance to the source. $I_1$ and $I_2$ are denoting the intensity at absorption maxima at $L_1$ and $L_2$ distance. Applying Eq. (A1), the intensity $I_2$ can be described in terms of $I_1$:

$$\begin{aligned} I_2 &= I_0 \cdot (1 - e^{-\epsilon \cdot L_2}) \\ &= I_1 + (I_0 - I_1)\,(1 - e^{-\epsilon \times \Delta L}) \end{aligned} \tag{A3}$$

where $\Delta L$ is the difference between $L_1$ and $L_2$. Thus $S(L_2)$ can be written as

$$ln\left(\frac{I_0}{I_2}\right) = ln\left(\frac{I_0}{I_1 + (I_0 - I_1)\,(1 - e^{-\epsilon \times \Delta L})}\right)$$

$$= ln\left(\frac{I_0}{I_0 + (I_1 - I_0) \times e^{-\epsilon \times \Delta L})}\right)$$
$$= -ln\left(\frac{I_0 + (I_1 - I_0) \times e^{-\epsilon \times \Delta L})}{I_0}\right)$$
$$= -ln\left(1 + \frac{I_1 - I_0}{I_0} \times e^{-\epsilon \times \Delta L}\right) \quad \text{(A4)}$$

The logarithm $ln(x)$ can be expressed as a Taylor series if $-1 < x < 1$ with

$$ln(x+1) = \sum_{k=1}^{\infty} (-1)^{k-1} \times \frac{x^k}{k} \quad \text{(A5)}$$

If $x$ is close to 0, the logarithm can be approximated by using only the first term ($ln\,(x+1) = x$). This means that Eq. (A4) can estimated by

$$S(L_1) \propto -\frac{I_1 - I_0}{I_0} \quad \text{(A6)}$$

$$S(L_2) \propto -\frac{I_1 - I_0}{I_0} \times e^{-\epsilon \times \Delta L} \quad \text{(A7)}$$

as long as $I_0 \approx I_1$, which is the case for a weak absorber. The relative change of SCD $S(L_1)$ to $S(L_2)$ with distance $\Delta L$ is given by

$$\frac{S(L_2)}{S(L_1)} = \frac{ln\left(\frac{I_0}{I_2}\right)}{ln\left(\frac{I_0}{I_1}\right)}$$
$$\approx \frac{\frac{I_1 - I_0}{I_0} \times e^{-\epsilon \times \Delta L}}{\frac{I_1 - I_0}{I_0}}$$
$$\approx e^{-\epsilon \times \Delta L} \quad \text{(A8)}$$



Thus Eq. (A8) can be used to estimate the dependence of DOAS measurements of a confined trace gas on distance between instrument and absorber. $\epsilon$ is an extinction coefficient, which depends on retrieval wavelength range and the absorption structure of the trace gas of interest in the respective retrieval wavelength range. E.g. depending on how the dominant absorption bands of the trace gas of interest are distributed within the retrieval wavelength range. Also, it must be stressed that above approximation is only valid for weak absorbers, because all but the the first term of Eq. (A5) are omitted.

*Acknowledgements.* The authors would like to thank the Mexican students who honorary helped with the ground based instruments. The measurements were performed in the frame of the FIEL-Volcan project, funded by the "Fondo de Cooperación Internacional de Ciencia y Tecnología Unión Europea México" (FONCICyT, CONACYT-EU) grant 93645.

## References

Ash Dispersal Forecast and Civil Aviation Workshop, Consensual Document, Geneva, Switzerland, 2010. 2832

Berglen, T. F., Berntsen, T. K., Isaksen, I. S. A., and Sundet, J. K.: A global model of the coupled sulfur/oxidant chemistry in the troposphere: The sulfur cycle, J. Geophys. Res., 109, D19310, doi:10.1029/2003JD003948, 2004. 2833

Bluth, G. J. S., Shannon, J. M., Watson, I. M., Prata, A. J., and Realmuto, V. J.: Development of an ultra-violet digital camera for volcanic $SO_2$ imaging, J. Volcanol. Geoth. Res., 161, 47–56, doi:10.1016/j.jvolgeores.2006.11.004, 2007. 2834, 2849, 2853

Bogumil, K., Orphal, J., Homann, T., Voigt, S., Spietz, P., Fleischmann, O., Vogel, A., Hartmann, M., Kromminga, H., Bovensmann, H., Frerick, J., and Burrows, J.: Measurements of molecular absorption spectra with the SCIAMACHY pre-flight model: instrument characterization and reference data for atmospheric remote-sensing in the 230–2380 nm region, J. Photoch. Photobi. A, 157, 167–184, doi:10.1016/S1010-6030(03)00062-5, 2003. 2840

Carn, S. A., Krueger, A. J., Krotkov, N. A., Yang, K., and Evans, K.: Tracking volcanic sulfur dioxide clouds for aviation hazard mitigation, Nat. Hazards, 51, 325–343, doi:10.1007/s11069-008-9228-4, 2009. 2833

Casadevall, T.: The 1989–1990 eruption of Redoubt volcano, Alaska – Impact on aircraft operations, J. Volcanol. Geoth. Res., 62, 301–316, 1994. 2830

Clarisse, L., Prata, F., Lacour, J.-L., Hurtmans, D., Clerbaux, C., and Coheur, P.-F.: A correlation method for volcanic ash detection using hyperspectral infrared measurements, Geophys. Res. Lett., 37, L19806, doi:10.1029/2010GL044828, 2010. 2832, 2833

Dalton, M. P., Watson, I. M., Nadeau, P. A., Werner, C., Morrow, W., and Shannon, J. M.: Assessment of the UV camera sulfur dioxide retrieval for point source plumes, J. Volcanol. Geoth. Res., 188, 358–366, doi:10.1016/j.jvolgeores.2009.09.013, 2009. 2834

Deutschmann, T.: Atmospheric radiative transfer modelling using Monte Carlo methods, Master's thesis, University Heidelberg, 2008. 2841

Deutschmann, T., Beirle, S., Friess, U., Grzegorski, M., Kern, C., Kritten, L., Platt, U., Prados-Roman, C., Pukite, J., Wagner, T., Werner, B., and Pfeilsticker, K.: The Monte Carlo atmospheric radiative transfer model McArtim: Introduction and validation of Jacobians and 3D features, J. Quant. Spectrosc. Ra., 112, 1119–1137, doi:10.1016/j.jqsrt.2010.12.009, 2011. 2841

Doasis: DOAS Intelligent System, Institute of Environmental Physics, University Heidelberg, Germany, Version 3.2.3799.23257, https://doasis.iup.uni-heidelberg.de/bugtracker/projects/doasis/, 2010. 2840

Doran, J., Abbott, S., Archuleta, J., Bian, X., Chow, J., Coulter, R., de Wekker, S., Edgerton, S., Elliott, S., Fernandez, A., Fast, J., Hubbe, J., King, C., Langley, D., Leach, J., Lee, J., Martin, T., Martinez, D., Martinez, J., Mercado, G., Mora, V., Mulhearn, M., Pena, J., Petty, R., Porch, W., Russell, C., Salas, R., Shannon, J., Shaw, W., Sosa, G., Tellier, L., Templeman, B., Watson, J., White, R., Whiteman, C., and Wolfe, D.: The IMADA-AVER boundary layer experiment in the Mexico City area, B. Am. Meteorol. Soc., 79, 2497–2508, 1998. 2834

Galle, B., Johansson, M., Rivera, C., Zhang, Y., Kihlman, M., Kern, C., Lehmann, T., Platt, U., Arellano, S., and Hidalgo, S.: Network for Observation of Volcanic and Atmospheric Change (NOVAC) – A global network for volcanic gas monitoring: Network layout and instrument description, J. Geophys. Res.-Atmos., 115, D05304, doi:10.1029/2009JD011823, 2010. 2837, 2839, 2876

Grindle, T. and Burcham, F.: Engine Damage to a NASA DC-8-72 Airplane From a High-Altitude Encounter With a Diffuse Volcanic Ash Cloud, Tech. rep., NASA, Dryden Flight Research Center, http://ntrs.nasa.gov/archive/nasa/casi.ntrs.nasa.gov/20030068344_2003079762.pdf, 2003. 2830



Guffanti, M., Schneider, D. J., Wallace, K. L., Hall, T., Bensimon, D. R., and Salinas, L. S.: Aviation response to a widely dispersed volcanic ash and gas cloud from the August 2008 eruption of Kasatochi, Alaska, USA, J. Geophys. Res., 115, D00L19, doi:10.1029/2010JD013868, 2010. 2833

Heue, K.-P., Brenninkmeijer, C. A. M., Baker, A. K., Rauthe-Schöch, A., Walter, D., Wagner, T., Hörmann, C., Sihler, H., Dix, B., Frie, U., Platt, U., Martinsson, B. G., van Velthoven, P. F. J., Zahn, A., and Ebinghaus, R.: $SO_2$ and BrO observation in the plume of the Eyjafjallajökull volcano 2010: CARIBIC and GOME-2 retrievals, Atmos. Chem. Phys., 11, 2973–2989, doi:10.5194/acp-11-2973-2011, 2011. 2835

ICAO: Manual on Volcanic Ash, Radioactive Material, and Toxic Chemical Clouds, 2nd Edition, International Civil Aviation Organization, 2 Edn., http://www.paris.icao.int/news/pdf/9691.pdf, doc 9691-AN/954, 2007. 2830, 2831, 2832

Johansson, M., Galle, B., Zhang, Y., Rivera, C., Chen, D., and Wyser, K.: The dual-beam mini-DOAS technique-measurements of volcanic gas emission, plume height and plume speed with a single instrument, B. Volcanol., 71, 747–751, doi:10.1007/s00445-008-0260-8, 2009. 2837

Kantzas, E. P., McGonigle, A. J. S., Tamburello, G., Aiuppa, A., and Bryant, R. G.: Protocols for UV camera volcanic $SO_2$ measurements, J. VOLCANOL. Geoth. Res., 194, 55–60, doi:10.1016/j.jvolgeores.2010.05.003, 2010. 2834

Karagulian, F., Clarisse, L., Clerbaux, C., Prata, A. J., Hurtmans, D., and Coheur, P. F.: Detection of volcanic $SO_2$, ash, and $H_2SO_4$ using the Infrared Atmospheric Sounding Interferometer (IASI), J. Geophys. Res.-Atmos., 115, D00L02, doi:10.1029/2009JD012786, 2010. 2833

Kern, C., Kick, F., Lübcke, P., Vogel, L., Wöhrbach, M., and Platt, U.: Theoretical description of functionality, applications, and limitations of $SO_2$ cameras for the remote sensing of volcanic plumes, Atmos. Meas. Tech., 3, 733–749, doi:10.5194/amt-3-733-2010, 2010a. 2834

Kern, C., Deutschmann, T., Vogel, L., Woehrbach, M., Wagner, T., and Platt, U.: Radiative transfer corrections for accurate spectroscopic measurements of volcanic gas emissions, B. Volcanol., 72, 233–247, doi:10.1007/s00445-009-0313-7, 2010b. 2840

Khokhar, M., Frankenberg, C., Van Roozendael, M., Beirle, S., Kuhl, S., Richter, A., Platt, U., and Wagner, T.: Satellite observations of atmospheric $SO_2$ from volcanic eruptions during the time-period of 1996–2002, in: atmospheric remote sensing: earth's surface, troposphere, stratosphere and mesosphere – I, edited by: Burrows, J. P. and Eichmann, K. U., vol. 36

of Advances in space research, 879–887, Elsevier Science LTD, The Boulevard, Langford Lane, Kidlington, Oxford 0X5 1GB, Oxon, UK, doi:10.1016/j.asr.2005.04.114, 2005. 2833
Khokhar, M. F., Platt, U., and Wagner, T.: Temporal trends of anthropogenic $SO_2$ emitted by non-ferrous metal smelters in Peru and Russia estimated from Satellite observations, Atmos. Chem. Phys. Discuss., 8, 17393–17422, doi:10.5194/acpd-8-17393-2008, 2008. 2833
Kraus, S. G.: DOASIS, A Framework Design for DOAS, Ph.D. thesis, University of Mannheim, 2006. 2840
Krueger, A.: Sighting of El Chichon sulfur dioxide clouds with the Nimbus 7 total ozone mapping spectrometer, Science, 220, 1377–1379, 1983. 2833
Kurucz, R. L.: High resolution irradiance spectrum from 300 to 1000 nm, AFRL Transmission Meeting, Lexington, Mass, http://kurucz.harvard.edu/sun.html, 2005. 2840
Lehmann, T.: Improving the sensitivity of spectroscopic measurements of atmospheric trace gases by modern signal processing algorithms, Ph.D. thesis, IUP, University Heidelberg, in preparation, 2011. 2840
Louban, I., Bobrowski, N., Rouwet, D., Inguaggiato, S., and Platt, U.: Imaging DOAS for volcanological applications, B. Volcanol., 71, 753–765, doi:10.1007/s00445-008-0262-6, 2009. 2852
Lübcke, P.: Development of a new $SO_2$ camera for volcanic gas flux measurements, Master's thesis, Insitute of Environmental Science, University Heidelberg, 2010. 2834
Miller, T. and Casadevall, T.: Encyclopedia of volcanoes, chap. Volcanic ash hazards to aviation, Academic Press, San Diego, USA, 2000. 2830
Mori, T. and Burton, M.: The SO2 camera: A simple, fast and cheap method for ground-based imaging of SO2 in volcanic plumes, Geophys. Res. Lett., 33, L24804, doi:10.1029/2006GL027916, 2006. 2834
Mori, T., Mori, T., Kazahaya, K., Ohwada, M., Hirabayashi, J., and Yoshikawa, S.: Effect of UV scattering on $SO_2$ emission rate measurements, Geophys. Res. Lett., 33, L17315, doi:10.1029/2006GL026285, 2006. 2840
Pavolonis, M. and Sieglaff, J.: GOES-R Advanced Baseline Imager (ABI) Algorithm Theoretical Basis Document For Volcanic Ash (Detection and Height), Tech. rep., STAR, NESDIS, NOAA, Camp Springs, Maryland, USA, http://www.goes-r.gov/products/ATBDs/volcanic_ash.pdf, 2010. 2832
Pavolonis, M. J., Feltz, W. F., Heidinger, A. K., and Gallina, G. M.: A daytime complement to the reverse absorption technique for improved automated detection of volcanic ash, J. Atmos.



Ocean. Tech., 23, 1422–1444, 2006. 2832
Platt, U. and Stutz, J.: Differential Optical Absorption Spectroscopy: Principles and Application, Springer, doi:10.1007/978-3-540-75776-4, 2008. 2833, 2840, 2841, 2849, 2853
Prata, A.: Infrared radiative-transfer calculations for volcanic ash clouds, Geophys. Res. Lett., 16, 1293–1296, 1989. 2832, 2833
Prata, A. J.: Satellite detection of hazardous volcanic clouds and the risk to global air traffic, Nat. Hazards, 51, 303–324, doi:10.1007/s11069-008-9273-z, 2009. 2832
Prata, A. J. and Bernardo, C.: Retrieval of volcanic SO2 column abundance from atmospheric infrared sounder data, J. Geophys. Res.-Atmos., 112, D20204, doi:10.1029/2006JD007955, 2007. 2833
Prata, A. J. and Bernardo, C.: Retrieval of volcanic ash particle size, mass and optical depth from a ground-based thermal infrared camera, J. Volcanol. Geoth. Res., 186, 91–107, doi:10.1016/j.jvolgeores.2009.02.007, 2009. 2834
Prata, A. J. and Tupper, A.: Aviation hazards from volcanoes: the state of the science, Nat. Hazards, 51, 239–244, doi:10.1007/s11069-009-9415-y, 2009. 2830
Prata, A., Barton, I., Johnson, R., Kamo, K., and Kingwell, J.: Hazard from volcanic ash, Nature, 354, p. 25, 1991. 2834
Prata, F., Bluth, G., Rose, B., Schneider, D., and Tupper, A.: Failures in detecting volcanic ash from a satellite-based technique – Comments, Remote Sens. Environ., 78, 341–346, 2001. 2833
Prata, A., Rose, W., Self, S., and OBrien, D.: Global, long-term sulphur dioxide measurements from the TOVS data: a new tool for studying explosive volcanism and climate, Geophys. Monogr., 139, 75–92, 2003. 2833
READY: Real-time Environmental Applications and Display sYstem, , Air Resources Laboratory, NOAA, http://ready.arl.noaa.gov/READY.php, last access: January 2011. 2840
Realmuto, V., Abrams, M., Buongiorno, M., and Pieri, D.: The use of multispectral thermal infrared image data to estimate the sulfur-dioxide flux from volcanos – A case-study from Mount Etna, Sicily, July 29, 1986, J. Geophys. Res.-Sol. Ea., 99, 481–488, 1994. 2833
Rix, M., Valks, P., Hao, N., van Geffen, J., Clerbaux, C., Clarisse, L., Coheur, P.-F., Loyola R, D. G., Erbertseder, T., Zimmer, W., and Emmadi, S.: Satellite Monitoring of Volcanic Sulfur Dioxide Emissions for Early Warning of Volcanic Hazards, IEEE J. Sel. Top. Appl., 2, 196–206, doi:10.1109/JSTARS.2009.2031120, 2009. 2833
Romero, R. (Ed.): The International Airways Volcano Watch (IAVW). Proceedings of 2nd Inter-

national Conference on Volcanic Ash and Aviation Safety, Virginia,USA, 2004. 2832
Rose, W., Delene, D., Schnelder, D., Bluth, G., Krueger, A., Sprod, I., Mckee, C., Davies, H., and Ernst, G.: Ice in the 1994 Rabaul eruption cloud – implications for volcanic hazard and atmospheric effects, Nature, 375, 477–479, 1995. 2833
Schumann, U., Weinzierl, B., Reitebuch, O., Schlager, H., Minikin, A., Forster, C., Baumann, R., Sailer, T., Graf, K., Mannstein, H., Voigt, C., Rahm, S., Simmet, R., Scheibe, M., Lichtenstern, M., Stock, P., Rüba, H., Schäuble, D., Tafferner, A., Rautenhaus, M., Gerz, T., Ziereis, H., Krautstrunk, M., Mallaun, C., Gayet, J.-F., Lieke, K., Kandler, K., Ebert, M., Weinbruch, S., Stohl, A., Gasteiger, J., Gro, S., Freudenthaler, V., Wiegner, M., Ansmann, A., Tesche, M., Olafsson, H., and Sturm, K.: Airborne observations of the Eyjafjalla volcano ash cloud over Europe during air space closure in April and May 2010, Atmos. Chem. Phys., 11, 2245–2279, doi:10.5194/acp-11-2245-2011, 2011. 2833
Simpson, J., Hufford, G., Pieri, D., and Berg, J.: Failures in detecting volcanic ash from satellite-based technique, Remote Sens. Environ., 72, 191–217, 2000. 2833
Solomon, S., Schmeltekopf, A. L., and Sanders, R. W.: On the interpretation of zenith sky absorption measurements, J. Geophys. Res., 92, 8311–8319, 1987. 2840
Thomas, H. E. and Watson, I. M.: Observations of volcanic emissions from space: current and future perspectives, Nat. Hazards, 54, 323–354, doi:10.1007/s11069-009-9471-3, 2010. 2832
Tupper, A., Textor, C., Herzog, M., Graf, H.-F., and Richards, M. S.: Tall clouds from small eruptions: the sensitivity of eruption height and fine ash content to tropospheric instability, Nat. Hazards, 51, 375–401, doi:10.1007/s11069-009-9433-9, 2009. 2832
Voigt, S., Orphal, J., Bogumil, K., and Burrows, J.: The temperature dependence (203–293 K) of the absorption cross sections of O-3 in the 230-850 nm region measured by Fourier-transform spectroscopy, J. Photoch. Photobio. A, 143, 1–9, 2001. 2840
Wagner, T., Burrows, J. P., Deutschmann, T., Dix, B., von Friedeburg, C., Frie, U., Hendrick, F., Heue, K.-P., Irie, H., Iwabuchi, H., Kanaya, Y., Keller, J., McLinden, C. A., Oetjen, H., Palazzi, E., Petritoli, A., Platt, U., Postylyakov, O., Pukite, J., Richter, A., van Roozendael, M., Rozanov, A., Rozanov, V., Sinreich, R., Sanghavi, S., and Wittrock, F.: Comparison of box-air-mass-factors and radiances for Multiple-Axis Differential Optical Absorption Spectroscopy (MAX-DOAS) geometries calculated from different UV/visible radiative transfer models, Atmos. Chem. Phys., 7, 1809–1833, doi:10.5194/acp-7-1809-2007, 2007. 2841
Wen, S. and Rose, W.: Retrieval of sizes and total masses of particles in volcanic clouds using



AVHRR bands 4 and 5, J. Geophys. Res., 99, 5421–5431, 1994. 2832
Zehner, C. (Ed.): Monitoring Volcanic Ash from Space. Proceedings of the ESA-EUMETSAT workshop on the 14 April to 23 May 2010 eruption at the Eyjafjoll volcano, South Iceland, vol. ESA Publikation STM-280, ESA, ESA, Frascati, Italy, doi:10.5270/atmch-10-01, 2010. 2831
Zhang, Y. and Johansson, M.: MobileDOAS, Department of Earth and Space Sciences, Chalmers University of Technology, Gothenburg, Sweden, 2007. 2839

**Table 1.** Spectrographs used for airborne measurements, their respective viewing direction in mrad from centre and detection limits (95 % = 2×$\sigma$). $\sigma$ is the mean error of all measurements with distance greater than 10 km to the plume of approaches III-V for the respective instrument.

| Spectrograph model | viewing direction [mrad] | | $SO_2$ [$10^{16}$ molec cm$^{-2}$] detec. limit | $\sigma$ |
|---|---|---|---|---|
| QE65000 | 0 | centre | 1.6 | 0.8 |
| S2000 | 40 | up | 2.9 | 1.5 |
| S2000 | 40 | down | 2.8 | 1.4 |
| S2000 | 40 | port | 2.6 | 1.3 |
| S2000 | 40 | starboard | 2.9 | 1.4 |





**Table 2.** Mean altitude a.s.l. and azimuth direction from north for all plane approaches. Approaches marked by (*) are not used for the study e.g. due to variability in flight direction during approach or insufficient distance to the plume. Approach II ($^+$) with stable flight vector inside the plume is only used for camparison between ground based and airborne measurements (Sect. 4.1).

| Approach | Time [UTC] | Altitude [m] | Azimuth [°N] |
|---|---|---|---|
| I* | 15:58–16:03 | 5067 | 297 |
| II$^+$ | 16:06–16:11 | 5184 | 124 |
| III | 16:15–16:21 | 5197 | 334 |
| IV | 16:24–16:31 | 5186 | 174 |
| V | 16:42–16:49 | 5207 | 293 |
| VI* | 17:09–17:13 | 5546 | 314 |

**Table 3.** $SO_2$ concentrations, AEC and corresponding visibilities of the plume for different type A model runs. For further details see text.

| Model run | A1 | A2 | A3 |
|---|---|---|---|
| $SO_2$ [$10^{12}$ molec cm$^{-3}$] | 1.54 | 1.54 | 0.77 |
| AEC [km$^{-1}$] | 1 | 10 | 40 |
| Visibility [m] | 4000 | 400 | 100 |





**Table 4.** Results from the fits of function (2) to approaches III–V.

| Approach | | III | IV | V | Mean |
|---|---|---|---|---|---|
| $\epsilon$ | [$10^{-5}$] | 7.13 | 7.50 | 7.37 | 7.33 |
| conf $\epsilon$ | [$10^{-6}$] | 8.1 | 3.0 | 4.7 | 5.3 |
| A | [$10^{17}$] | 2.14 | 2.34 | 2.04 | 2.18 |
| conf A | [$10^{16}$] | 2.0 | 1.0 | 1.2 | 1.4 |
| $r^2$ | | 0.89 | 0.97 | 0.95 | 0.94 |

**Table 5.** Results from the fits to the radiative transfer models. $\epsilon$ and the $\pm\Delta$ to calculate confidence bands of 95 % (conf $\epsilon$) are given in [$10^{-5}$].

| Modell run | | A1 | A2 | A3 | Mean |
|---|---|---|---|---|---|
| 306.6 nm | $\epsilon$ | 9.08 | 7.63 | 7.14 | 7.95 |
| | conf $\epsilon$ | 0.166 | 0.089 | 0.136 | 0.130 |
| | $r^2$ | 0.9994 | 0.9998 | 0.9994 | 0.9995 |
| 310.8nm | $\epsilon$ | 7.80 | 6.65 | 6.24 | 6.89 |
| | conf $\epsilon$ | 0.083 | 0.105 | 0.144 | 0.111 |
| | $r^2$ | 0.9998 | 0.9996 | 0.9991 | 0.9995 |





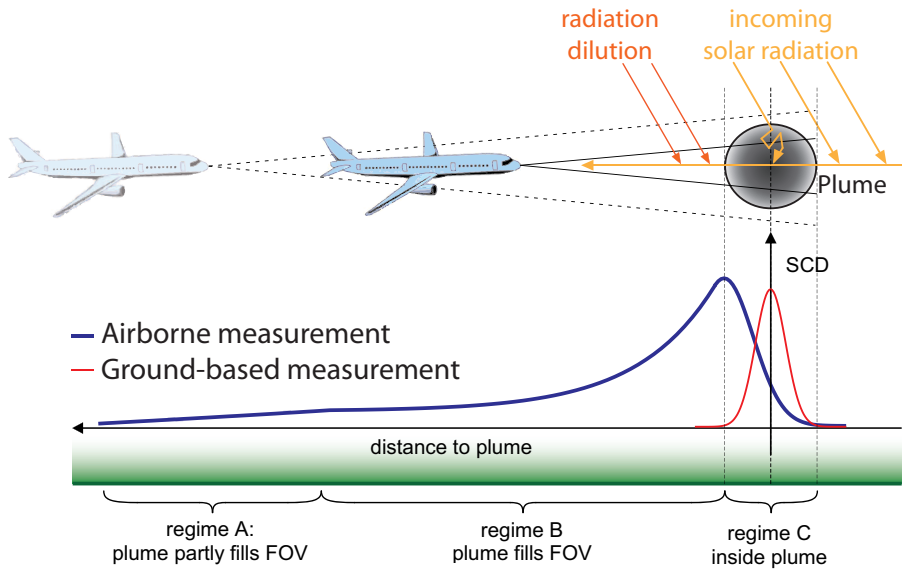


**Fig. 1.** Upper part: sketch of observation geometry of a forward looking telescope in an aircraft approaching a volcanic plume. There are three regimes: A – the plume only partly fills the field of view (FOV) of the instrument, B – the plume completely fills the FOV, C – the instrument is inside the plume. Lower part: $SO_2$ SCD seen by aircraft based (blue line) and ground based instruments (red line). Details see text.


**Fig. 2.** A schematic of the different airborne viewing directions. All telescopes were mounted at the airplane close to co-pilots window. The viewing directions (up, down, starboard, port) were looking at angles of 40 mrad with respect to centre and a horizontal plane (up, down) or a vertical plane (starboard, port).





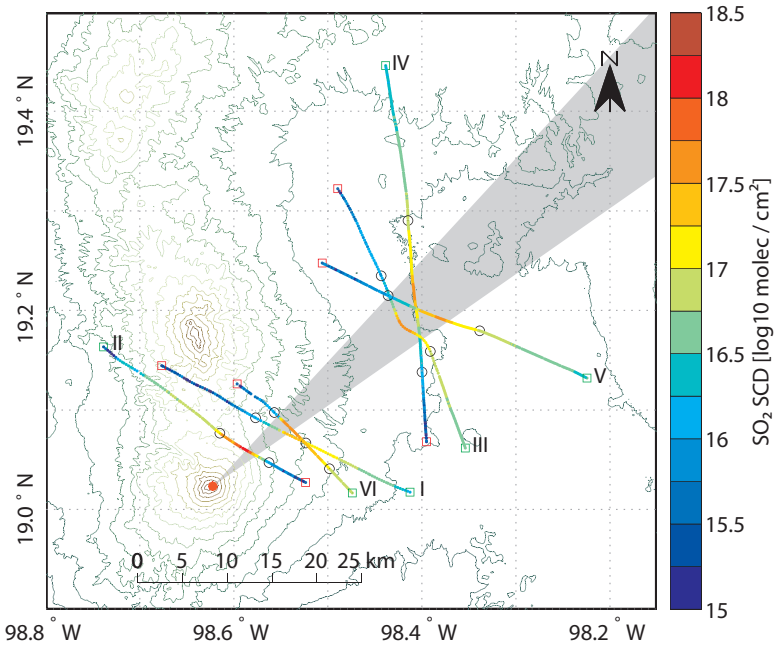


**Fig. 3.** Map of all six flown approaches. The start of each approach is marked by a green square, the end by a red square. The roman numbers next to the starting point correspond to the order of the different approaches. Note the logarithmic colour scale of the $SO_2$ SCDs. Popocatépetl is indicated with an orange dot at the lower left corner and its plume by the grey shaded area.

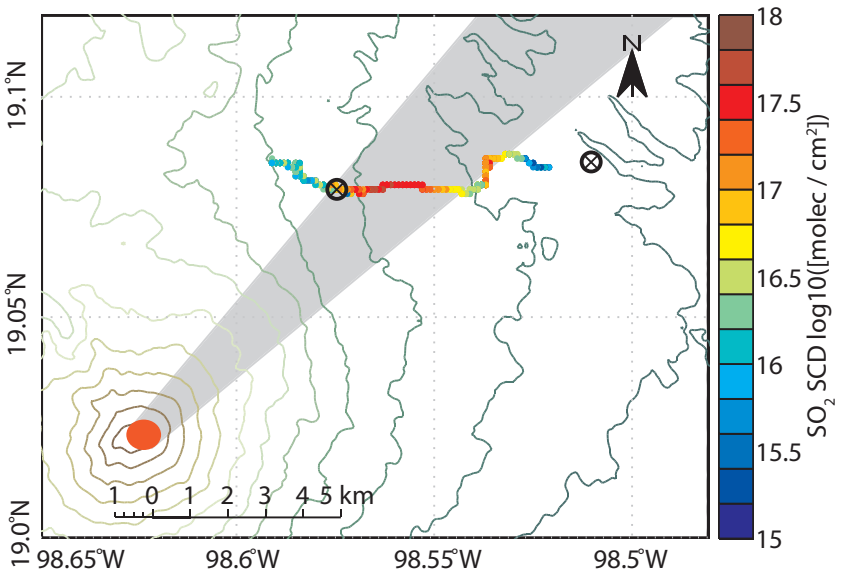


**Fig. 4.** Ground based measurements: An example of conducted car traverses is shown with measured $SO_2$ SCDs on a logarithmic scale. The locations of the stationary scanning instruments are marked by black circles. Popocatépetl as a source is indicated with an orange dot at the lower left corner and its plume by the grey shaded area.





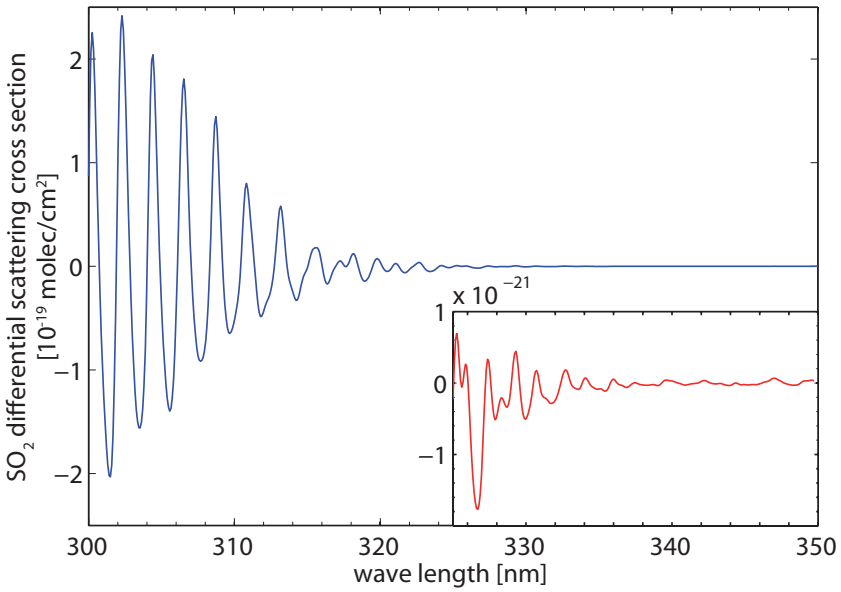


**Fig. 5.** A high pass filtered $SO_2$ cross section at the same optical resolution as the QE65000 spectrograph used with the centre looking telescope. The inserted graph displays the respective part of the $SO_2$ cross section magnified by a factor of 100.

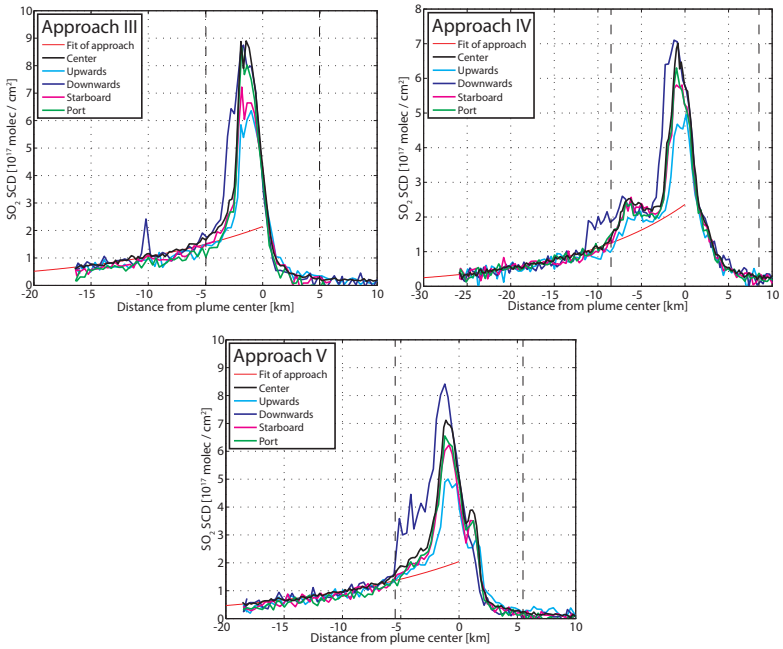


**Fig. 6.** Results from approaches III–V. The solid red lines indicate the fit of Eq. (2) to the measurement results in the far field. Dashed vertical lines indicate regime C. Errors of measurements are given in Table 1. $SO_2$ was detected from the first measurements onwards. Significant differences between the retrieved SCDs of the telescopes can not be distinguished for measurements at greater distance to the plume due the inferior signal-to-noise ratio of the Ocean Optics S2000 spectrometers (up, down, starboard, port viewing directions). Still, an vertical extension of the volcanic plume of at least 2 km can be deduced from the measurements at different vertical directions.



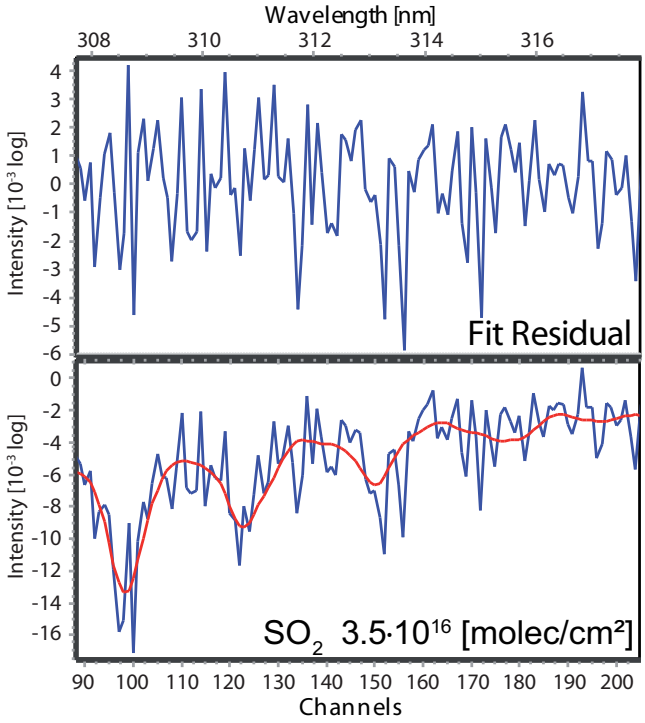


**Fig. 7.** Fit result for the the first spectrum in approach IV, taken at 25 km distance. Shown is the residual above and the fitted $SO_2$ SCD of $3.5 \times 10^{16}$ molec cm$^{-2}$ below.

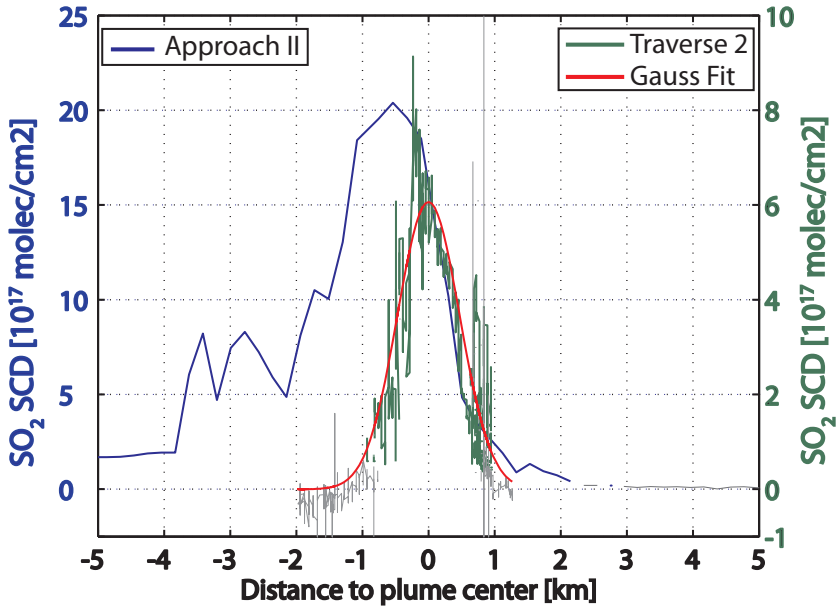


**Fig. 8.** Comparison of results from car traverses and airborne measurements, with scale of measured $SO_2$ SCDs on the right and left ordinate, respectively. Values below 3x measurement error are drawn in grey. Strong variations in the car traverse (e.g. at 1 km from plume centre) are artefacts due to vegetation blocking the view. The gradients shown agree with expected characteristics of transition between regime B to regime C (see Fig. 1), although the starting point of the plume of the car traverse does not correlate with the maximum of the values retrieved from the airborne measurement.



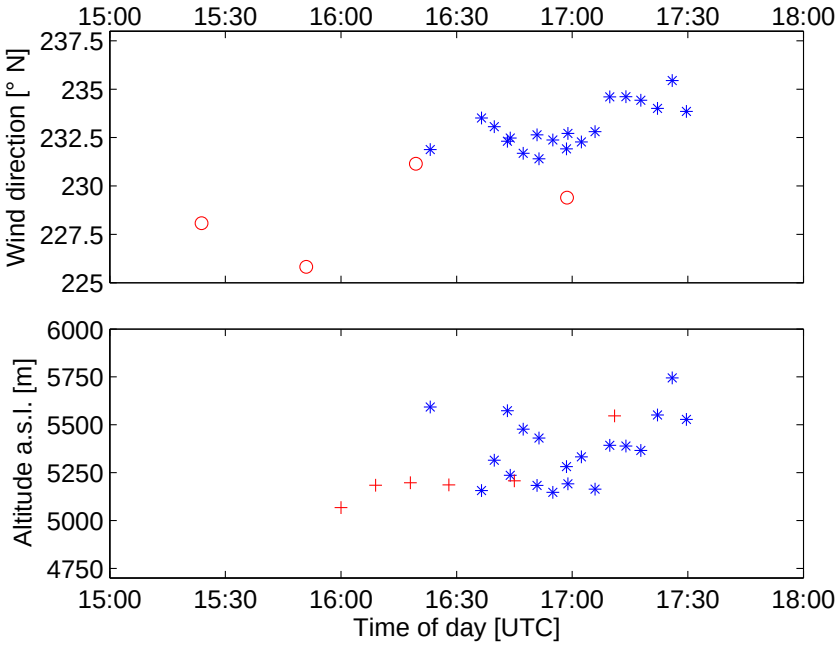


**Fig. 9.** Wind direction and altitude of plume centre derived from the ground based measurements, showing the stable meteorological conditions on 24 April 2010. Values derived by the two stationary scanning instruments according to (Galle et al., 2010) are depicted as blue asterisks, red circles show results from the car traverses. Also the mean altitude of the airplane is indicated for all approaches by red pluses. Note that the different types of measurements were conducted at different distances to the plume, which could explain the slightly differing values.

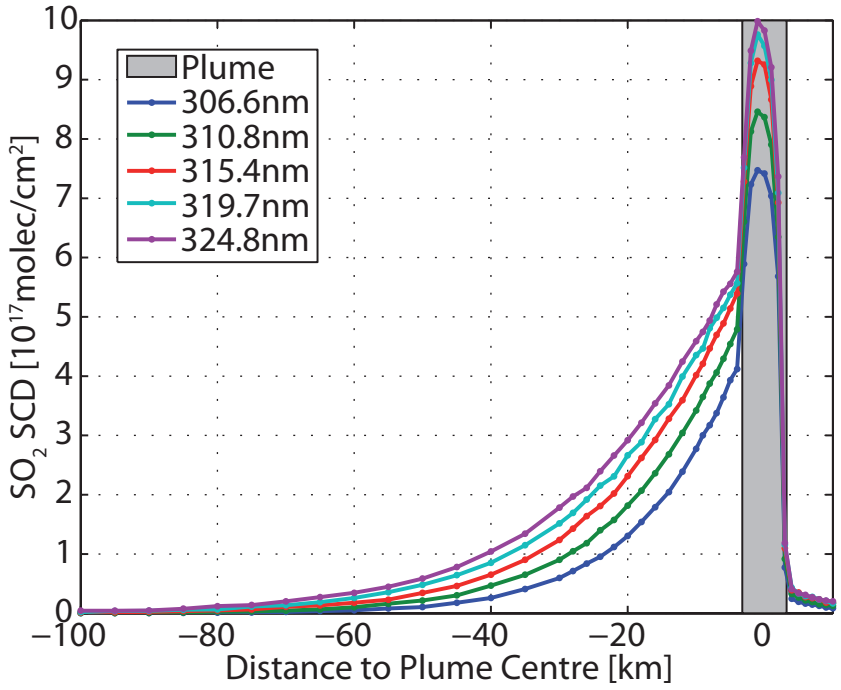


**Fig. 10.** The figure shows the results of model run A2. The AEC was set to 10 km$^{-1}$ corresponding to a visibility of 400 m inside the plume, which is marked as shaded area. The graph depicts simulated $SO_2$ column density as a function of the distance of the instrument from the plume.





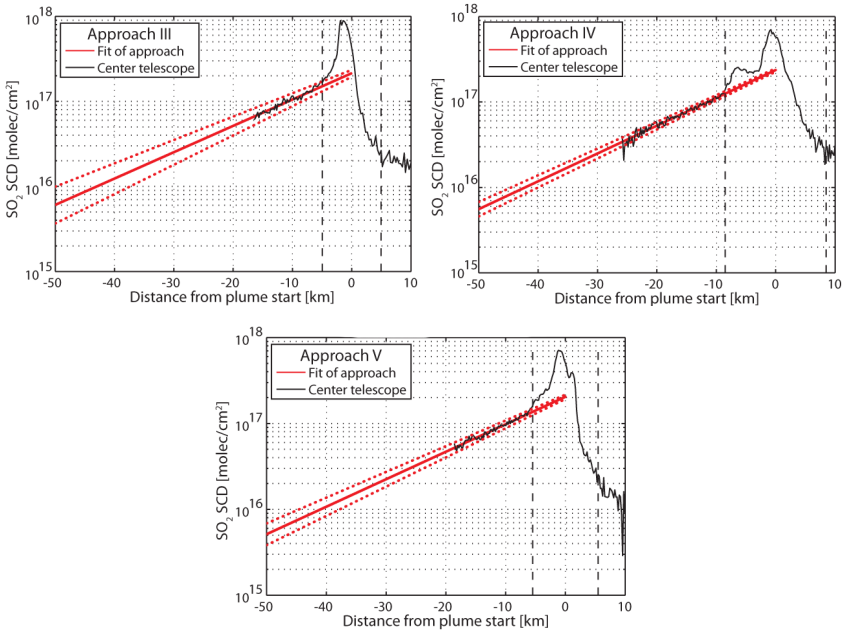


**Fig. 11.** Approaches III–V extrapolated to 50 km distance. Fitted function is depicted as red line with 95 % confidence bands as red dots. Measurement regime C is indicated by dashed vertical lines.

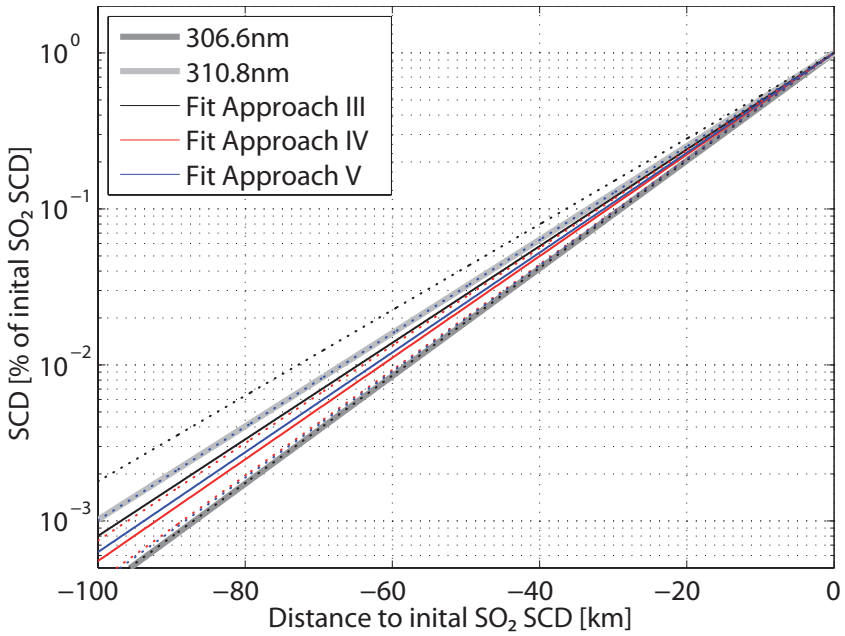


**Fig. 12.** Relative changes of $SO_2$ SCDs for approaches III–V and comparison to the mean extinction coefficients derived by model runs A1–A3. The dashed lines indicate the 95 % confidence interval.





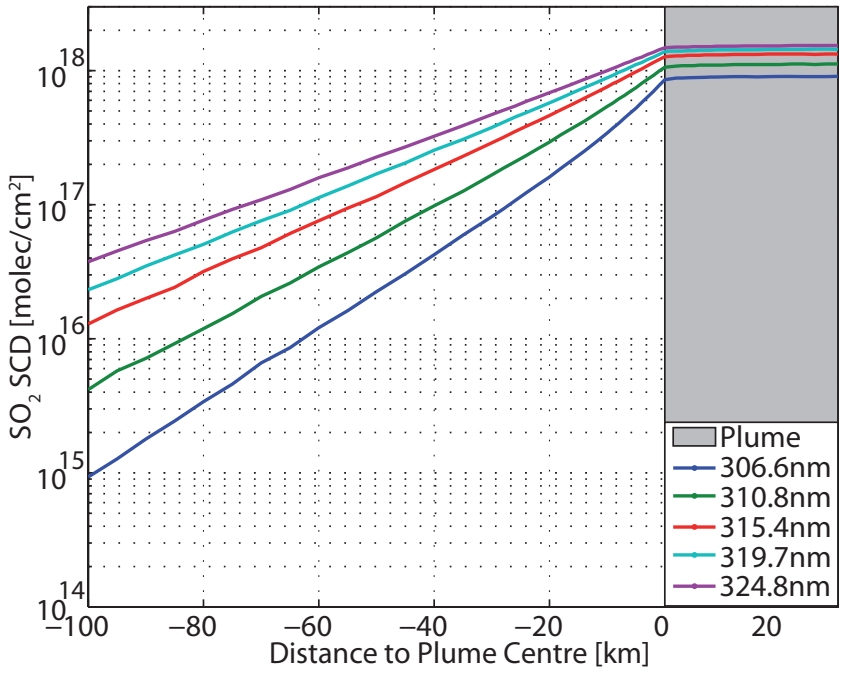


**Fig. 13.** Simulated $SO_2$ SCD from model scenario B3. Here, a volcanic cloud with infinite extent in propagation direction and from the edge onwards was assumed to be at 10 km altitude. An $SO_2$ concentration of $1 \times 10^{12}$ molec cm$^{-2}$ is assumed for the simulation, and the cloud exhibited an aerosol optical depth of 0.1 km$^{-1}$.

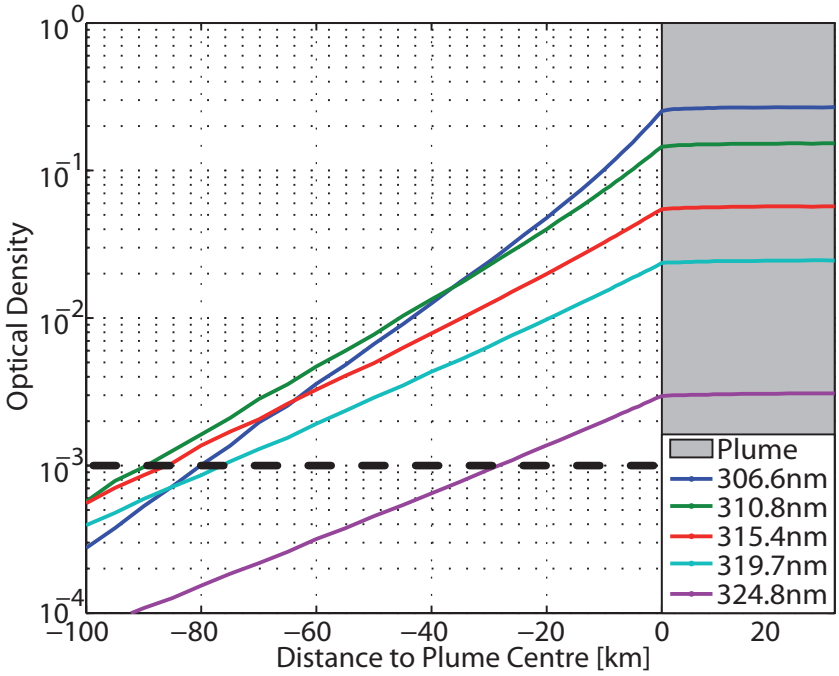


**Fig. 14.** In order to assess detectability of large scale volcanic cloud, the optical density are shown as calculated from model scenario B3. An optical density of more than $10^{-3}$ is obtained at distances greater than 80 km from the plume for the wavelength range 310–315 nm, thus indicating the possibility of a significantly earlier detection than is possible at lower altitudes.